Int. J. Electrochem. Sci., 15 **(2020)** 915 – 928, doi: 10.20964/2020.01.84

International Journal of
ELECTROCHEMICAL
SCIENCE
www.electrochemsci.org

A silicomolybdate/graphene/poly(3,4-Ethylenedioxythiophene) Composite Film as a Sensor for Sensitive Determination of Persulfate

Weihua Guo[1,2,*], *Jianguo Ma*[2], *Xiaohong Cao*[2], *Xiaolan Tong*[2], *Fen Liu*[2], *Yunhai Liu*[2,*]

[1] State Key Laboratory of Nuclear Resources and Environment, East China University of Technology, Nanchang, 330013, Jiangxi, China
[2] Chemistry, Biological and Materials Sciences Department, East China University of Technology, Nanchang, 330013, Jiangxi, China
[*]E-mail: guowh0604@163.com, whguo@ecit.cn, walton_liu@163.com

Received: 29 September 2019 / *Accepted:* 21 November 2019 / *Published:* 30 November 2019

A poly(3,4-ethylenedioxythiophene)-electrochemically reduced graphene oxide (pEDOT-ERGO) composite film was synthesized by one-step electropolymerization approach on the Indium tin oxide (ITO). The composite was further decorated with $H_4SiMo_{12}O_{40}$ ($SiMo_{12}$) by electrochemical growth method and applied as an electrode material for the detection of persulfate. pEDOT acted as a bridge in the composite because it is positively charged and can interact with the negatively charged species. Data from scanning electron microscopy (SEM), energy dispersive spectroscopy (EDS) and cyclic voltammetry demonstrated that the $SiMo_{12}$/pEDOT-ERGO film was successfully synthesized. The electrode surface has a granular-like protrusions structure and a large specific surface area. As a result of the catalytic activity of $SiMo_{12}$ and the good conductivity of pEDOT-ERGO, the modified electrode displays better electrocatalytic activity toward the reduction of persulfate. The sensor has a linear response in the 1.5-132 μM range with a detection limit (0.48 μM), better sensitivity (0.22 μA $\mu M^{-1} cm^{-2}$), favorable anti-interference and good stability.

Keywords: Graphene oxide, Polyoxometaltes, Poly(3,4-ethylenedioxythiophene), Persulfate, Electrocatalysis, Modified electrode

1. INTRODUCTION

As a strong oxidizing agent, persulfate has been employed as bleach, detergent, polymerization accelerator and so on. Finding a suitable method for detecting persulfate in water is significantly important, because it is harmful to human health (asthma and skin reactions, etc) [1, 2]. Several methods, e.g. HPLC [3], polarography [4] and spectrophotometriy [5], have been presented in the existing papers for the quantitative detection of persulfate. Among all analytical techniques established for quantitative

detection, electrochemical method is worth applying to use owing to its excellent sensitivity and selectivity. So far, a variety of electrode materials such as lead pentacyanonitrosylferrate [6], neutral red/nickel oxide nanowire [7], nano-ruthenium oxide/celestine blue [8], graphene quantum dots/riboflavin[9] have been applied to the detection of persulfate. Although acceptable conclusions have been obtained in most experiments, some of which are far from eco-friendly when using lead or dye composites.

Polyoxometalates (POMs), an inorganic metal oxide cluster compound, is a well-known redox material, and it has attracted more attention in the field of electrochemistry for detecting some small molecule, such as H_2O_2[10], NO_2^-[11], IO_3^-[12], dopamine and ascorbic acid[13]. However, direct application of POMs is a significant challenge because of its low specific surface area and high solubility in aqueous solution. In fact, these problems limit its application in electrochemical systems. To improve the stability and maximize electrocatalytic activity of POMs-based modified electrodes, a large number of materials have been selected to prepare POMs films, such as metal nano-objects, conducting polymers and carbon materials [14-17]. Among these, graphene stands out because of its interesting physicochemical properties [18, 19]. Indeed, graphene has large surface area and good conductivity, and these properties are very advantageous to design POMs-based composite nanomaterials. Nevertheless, easy agglomeration is a shortcoming of graphene. Studies have proved that graphene oxide (GO) has a unique advantage in the construction of graphene-POMs composites since it has good solubility in aqueous [20-24]. However, how to overcome the electrostatic repulsion between the negatively charged POMs and GO is also a challenge when they are combined.

Conducting polymers and their composite materials have been employed to improve the performance of electrochemical sensors. As a conducting polymer, Poly(3,4-ethylenedioxythiophene) (pEDOT) has been studied in the field of electrochemical sensor owing to its especial stability and high conductivity[25, 26]. Up to now, several works about pEDOT/graphene nanocomposites have been reported[27, 28]. Among these studies, pEDOT/graphene modified electrodes are normally fabricated by two different methods. The first method is to mix graphene directly with PEDOT-PSS, and the second method is in situ chemical or electrochemical polymerization of EDOT monomers on GO. The electrochemical polymerization method is advantageous to produce a relatively uniform pEDOT/graphene layer with changeable thickness. Moreover, it is noteworthy that the positively charged pEDOT can electrostatically interact with the negatively charged species, thus contributing to the combination of POMs and GO. In short, the introduction of pEDOT into graphene-POMs composites is meaningful.

In this study, we report a facile fabrication of $H_4SiMo_{12}O_{40}$ decorated pEDOT-electrochemically reduced graphene oxide, designated as $SiMo_{12}$/pEDOT-ERGO, by integrating the excellent electrocatalytic capacity of $SiMo_{12}$ with the out-standing conductivity of the pEDOT-ERGO nanocomposite film. Scheme 1 describes the synthetic route of the pEDOT-ERGO nanocomposite and its interaction with POM. First, the pEDOT-ERGO nanocomposite film was electropolymerized on the Indium tin oxide electrode (ITO) by cyclic voltammetry using GO and EDOT as the starting materials. Polymerization of EDOT monomers and electrochemical reduction of GO to graphene (ERGO) occur at different potentials during cyclic potential scanning. Then the pEDOT-ERGO nanocomposite film electrode was used for the immobilization of $SiMo_{12}$ by electrochemical growth method. The negatively

charged $SiMo_{12}$ adhered to the pEDOT-ERGO nanocomposite film by means of the electrostatic interaction between $SiMo_{12}$ and the positively charged pEDOT backbone. The pEDOT-ERGO not only played an important role in improving the surface area, but also accelerated electron transfer. Successful formation of $SiMo_{12}$/pEDOT-ERGO film was examined by scanning electron microscopy (SEM), energy dispersive spectroscopy (EDS) and cyclic voltammetry. The composite electrode presented good electrocatalytic activity toward the detection of persulfate with high sensitivity, low detection limit and better selectivity.

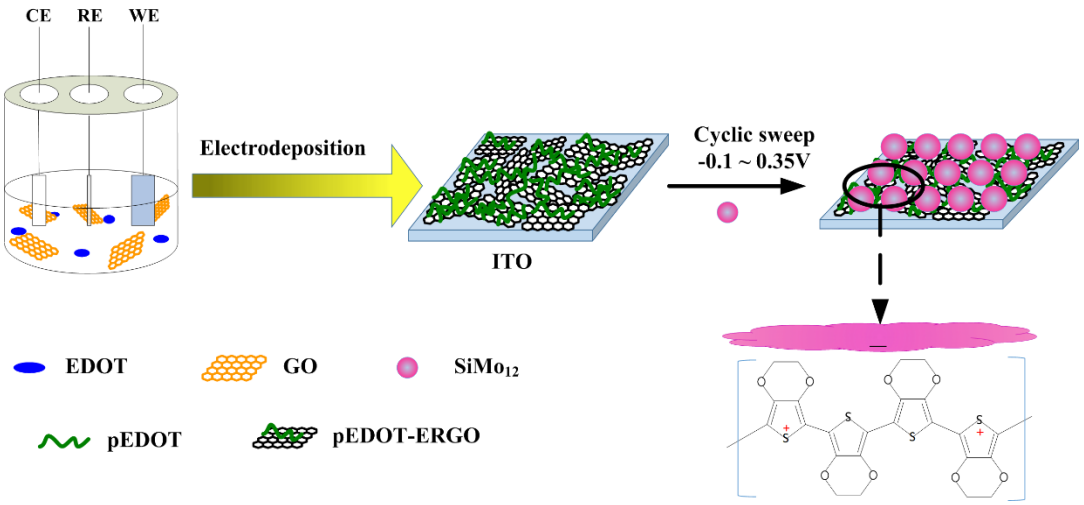

Scheme 1. Schematic illustration for the preparation of $SiMo_{12}$/pEDOT-ERGO electrode.

2. EXPERIMENTAL

2.1. Reagents and apparatus

3, 4-ethylenedioxythiophene (EDOT) and graphite (powder < 20 μm) were obtained from Sigma–Aldrich Company. Graphene oxide (GO) was synthesized according to the method of literature[29]. $H_4SiMo_{12}O_{40}\cdot xH_2O$ ($SiMo_{12}$) was synthesized in accordance with the previous report [30].

CHI660D Electrochemical Workstation with three-electrode system was used to perform the electrochemical experiments. $SiMo_{12}$/pEDOT-ERGO modified Indium tin oxide (ITO), Pt wire and saturated calomel electrode (SCE) were employed as working, counter and reference electrode, respectively. For the preparation of $SiMo_{12}$/pEDOT-ERGO/ITO, ITO was firstly cleaned according to the literature method [31]. Nava NanoSEM 450 field emission scanning electron microscope was used to visualize the scanning electron microscopic (SEM).

2.2. Preparation of ERGO, pEDOT and pEDOT-ERGO nanocomposite film

The pEDOT-ERGO modified ITO electrode was performed by cyclic voltammetry in 0.01 M KCl including 1.0 mg mL^{-1} GO and 0.01 M EDOT monomer. The potential cycling was carried out

between −1.5 and 1.1 V at 100 mV s^{-1} for 10 cycles. For comparison, the electrochemical polymerization of EDOT (pEDOT) in absence of GO was prepared by the same procedure in the potential window −0.9 to 1.1 V, and the ERGO/ITO was synthesized similar to the preparation of pEDOT-ERGO/ITO except for the addition of EDOT.

2.3 Preparation of $SiMo_{12}$ electrodes

The $SiMo_{12}$ was electrodeposited on the pEDOT-ERGO/ITO in 0.1 mM $SiMo_{12}$ at 50 mV s^{-1} for 25 scan cycles in the potential window −0.1 to 0.35 V. The $SiMo_{12}$ modified bare, ERGO or pEDOT/ITO was prepared by the similar manner.

3. RESULTS AND DISCUSSION

3.1 Fabrication and Morphology of $SiMo_{12}$/pEDOT-ERGO modified electrode

Controlled electrodeposition of ERGO film, pEDOT film or pEDOT-ERGO composite film was obtained by cyclic voltammetry in the respective modification mixtures detailed in the experimental section.

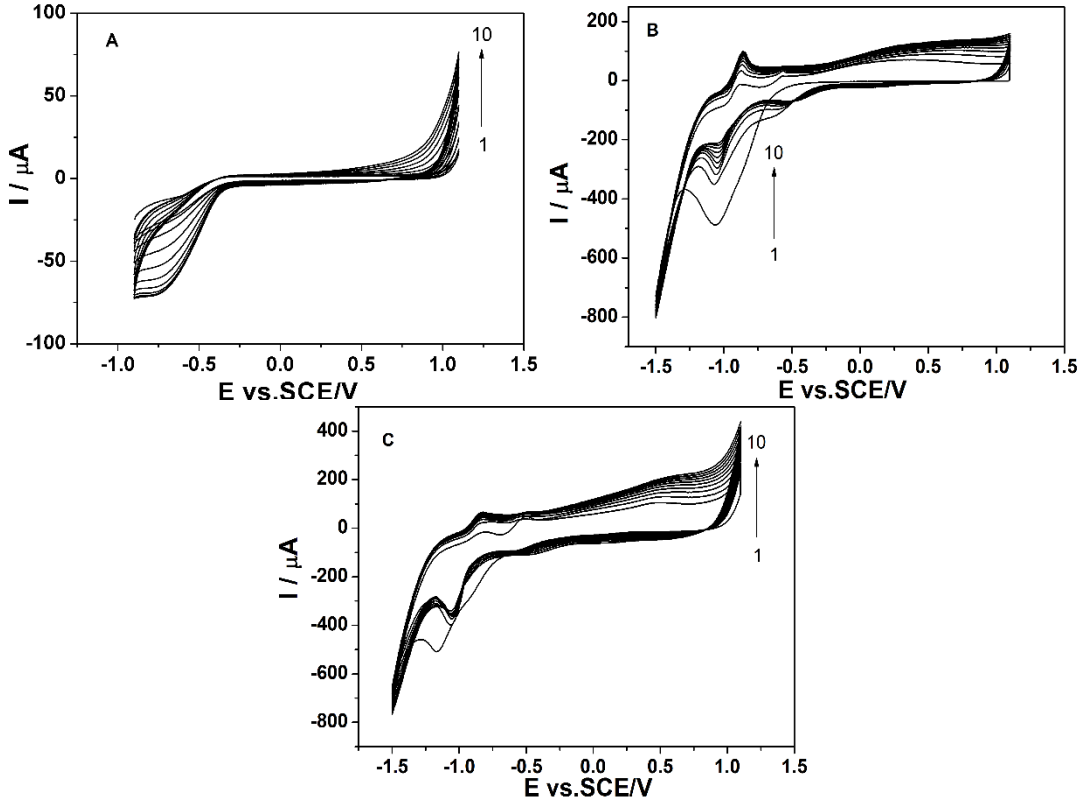

Figure 1. Cyclic voltammograms for the electrolysis of (A) 0.01 M EDOT, (B) 1.0 mg mL^{-1}GO and (C) 1.0 mg mL^{-1} GO + 0.01 M EDOT in 0.01 M KCl aqueous solutions at a scan rate of 100 mV s^{-1}.

Fig. 1 shows the growth of ERGO film, pEDOT film and pEDOT-ERGO composite film on the ITO electrode confirmed by the changes of peak currents, which is accordant with the previous reports [32] that pEDOT layers are produced on the electrode surface in the course of positive scans. Simultaneously, GO was attracted during potential cycling and then reduced to graphene [33].

The morphology of the as-prepared film was examined by SEM. Fig. 2 displays the SEM images of (A) $SiMo_{12}$, (B) $SiMo_{12}$/pEDOT, (C, D) $SiMo_{12}$/ERGO, (E, F) $SiMo_{12}$/pEDOT-ERGO coated ITO electrodes. The whole $SiMo_{12}$ film (Fig.2A) is relatively smooth, manifesting as a regular globular structure due to the aggregaion of $SiMo_{12}$ anions. In Fig. 2B, it is found that the size of the globular microstructure increases, which could be ascribed to the great aggregation of $SiMo_{12}$ anions on the pEDOT film. The morphology of the $SiMo_{12}$/ERGO is different from that of $SiMo_{12}$ and $SiMo_{12}$/pEDOT. Different magnification SEM images of $SiMo_{12}$/ERGO are shown in Fig. 2C and D. The $SiMo_{12}$/ERGO formed an interconnected porous structure with high roughness, which was formed by wrinkled paper sheets. Additionally, these results suggest that the employed electrochemical deposition method can effectively produce reduced graphene oxide. From Fig. 2E and F, the $SiMo_{12}$/pEDOT-ERGO film exhibits a continuous, granular-like protrusions structure. These results suggest that the combination of ERGO with pEDOT is formed during the process of electropolymerization. Moreover, the surface coverage of ERGO is increased by adding GO to EDOT solution, since more negative charged GO is needed to neutralize the positive charge on the polymer backbone. There is no doubt that such rough structure of the composite films would supply a large surface area to promote the adsorption of the $SiMo_{12}$ from the electrolyte to the surface of electrode, which is consistent with the results of electrochemical experiments.

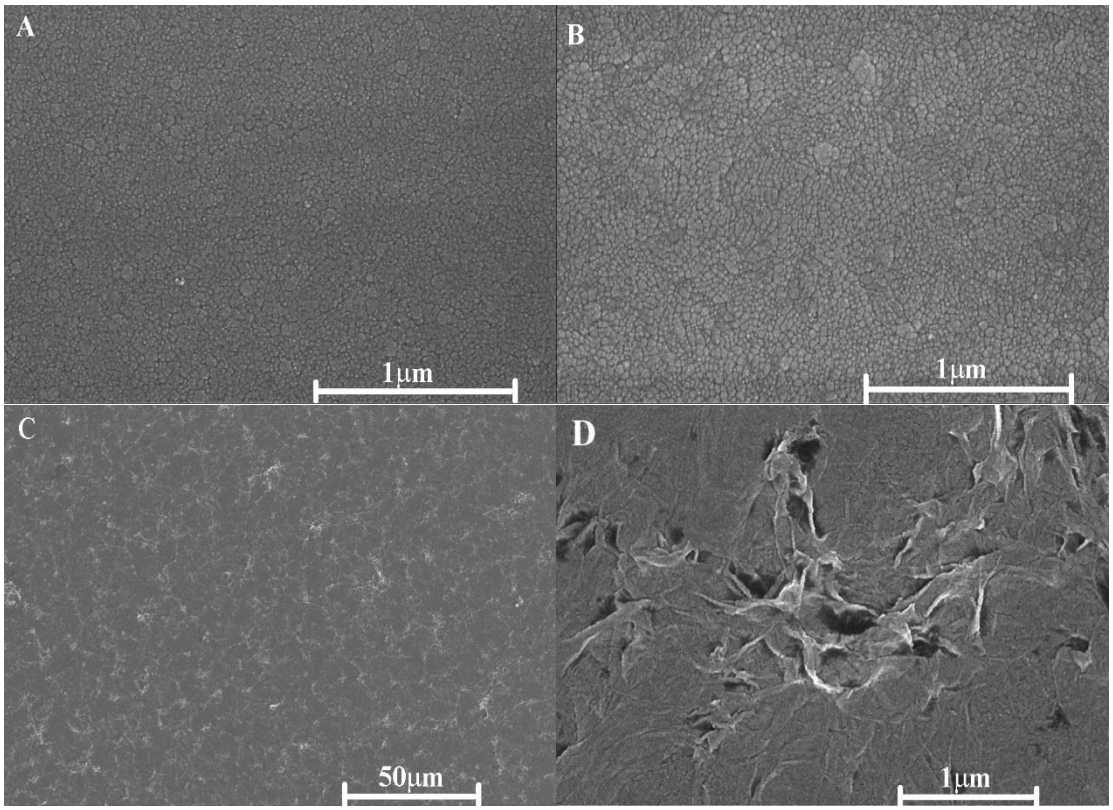

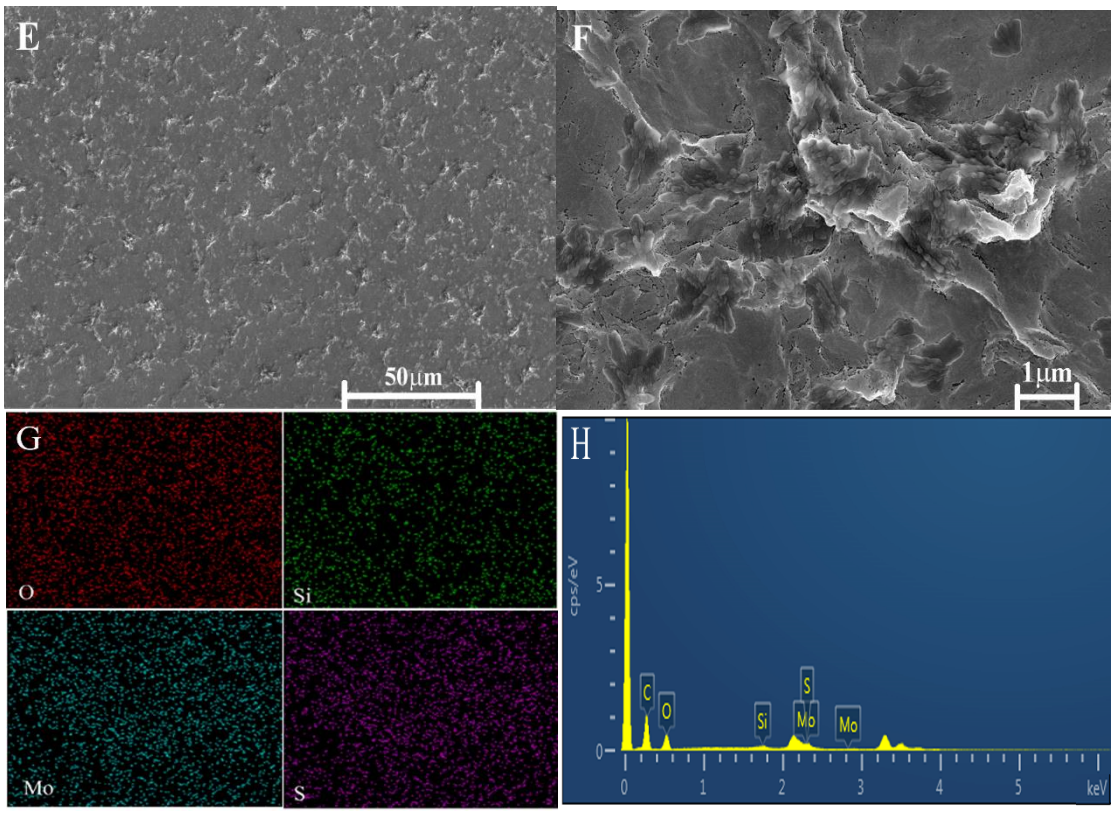

Figure 2. SEM images of (A) $SiMo_{12}$, (B) $SiMo_{12}$/pEDOT, (C,D) $SiMo_{12}$/ERGO, (E,F) $SiMo_{12}$/pEDOT-ERGO coated ITO electrodes. (G) and (H) EDS chemical constitution of the $SiMo_{12}$/pEDOT-ERGO composite film.

The EDS of the $SiMo_{12}$/pEDOT-ERGO film is shown in Fig. 2G and H. The noteworthy signals of C, O, Si, Mo and S, which are present in $SiMo_{12}$, ERGO and pEDOT, can be observed.

3.2 Electrochemical Characterisation of $SiMo_{12}$/pEDOT-ERGO modified electrode

Different material modified electrodes were characterized by cyclic voltammetry to study the synergistic effect of the pEDOT-ERGO. Fig. 3 presents the cyclic voltammograms obtained at ERGO/ITO, pEDOT/ITO and pEDOT-ERGO/ITO in 0.1 M KCl including 0.5 mM $Fe(CN)_6^{3-/4-}$ at 50 mV s^{-1}. Note that the peak current increases when ERGO (curve b) or pEDOT (curve c) is modified onto the ITO electrode (curve a), which indicates that ERGO or pEDOT increases electrochemical active sites. When the ERGO was incorporated into the pEDOT film (curve d), further increase of peak current could be observed. This should be attributed to the connection of conductive pEDOT and graphene, which effectively accelerated electron transfer rate, thus leading to synergic effect.

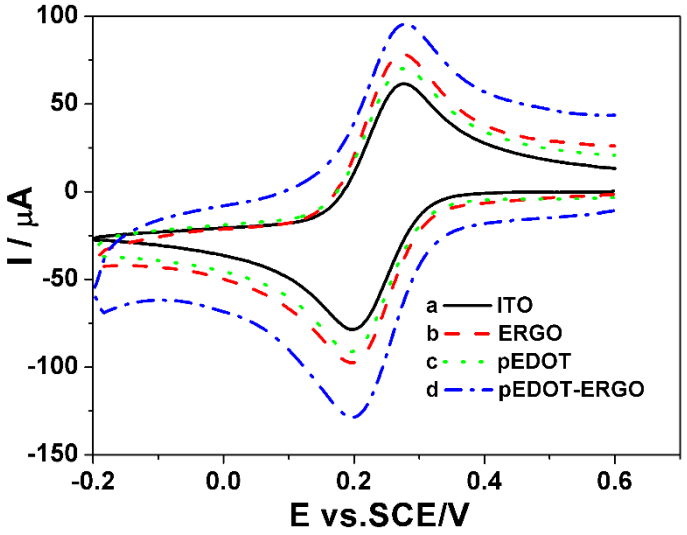

Figure 3. The cyclic voltammograms of the bare ITO (a), ERGO (b), pEDOT (c) and pEDOT-ERGO (d) electrodes in 0.5 mM $K_3Fe(CN)_6/K_4Fe(CN)_6$ (1:1) containing 0.1 M KCl at 50 mV s^{-1}.

According to Randles-Sevick formula, the efficient electrode surface area was calculated as follows: [34, 35]

$$I_p(A)=2.69\times10^5 n^{3/2} A D^{1/2} C \nu^{1/2} \quad (1)$$

where I_p (A) refers to the cathodic peak current, A is the electrode surface area (cm^2) and all other symbols have their usual meanings [36, 37]. By using eq 1, the active surface areas were found to be 0.94, 0.999, 1.055 and 1.312 cm^2 for bare ITO, ERGO, pEDOT and pEDOT-ERGOmodified electrode, respectively. These results reveal that the pEDOT-ERGO modified electrode has higher active surface area. The effective surface area of ERGO is just slightly higher than that of the bare ITO, which is related to the fact that graphene nanosheets are current parallel to collectors in the deposition process. In this case, the electroactive surface area can not be completely utilized because some of the regions are inaccessible to the electrolyte ions. Although the pEDOT is a good conductive polymer, the increase of its electrochemically active surface is still very limited. However, after incorporating ERGO into the pEDOT film, inorganic-organic hybrid materials were formed, which promoted the effective area of the modified electrode increases obviously. This indicates that ERGO could availably improve the coverage of pEDOT and enhance the surface area of the composite modified electrode, which could be advanatageous to load the electroactive materials.

Fig. 4 shows the cyclic voltammograms of (a) $SiMo_{12}$, (b) $SiMo_{12}$/ERGO, (c) $SiMo_{12}$/pEDOT, and (d) $SiMo_{12}$/pEDOT-ERGO modified ITO in 0.1 M sulphuric solution, respectively. There are three redox couples corresponding to $H_4SiMo_{12}O_{40}/H_6SiMo_{12}O_{40}$, $H_6SiMo_{12}O_{40}/H_8SiMo_{12}O_{40}$, and $H_8SiMo_{12}O_{40}/H_{10}SiMo_{12}O_{40}$ redox processes [1]. Compared with the $SiMo_{12}$/ITO, a significantly increased in peak current is clearly observed for $SiMo_{12}$/ERGO/ITO or $SiMo_{12}$/pEDOT/ITO. This phenomenon may be ascribed to the fact that presence of ERGO or pEDOT increases the surface concentration of $SiMo_{12}$. Evidently, the $SiMo_{12}$/pEDOT-ERGO/ITO shows the highest redox current in the four modified electrode, indicating that it has the maximum electroacitve surface area as well as the amount of $SiMo_{12}$.

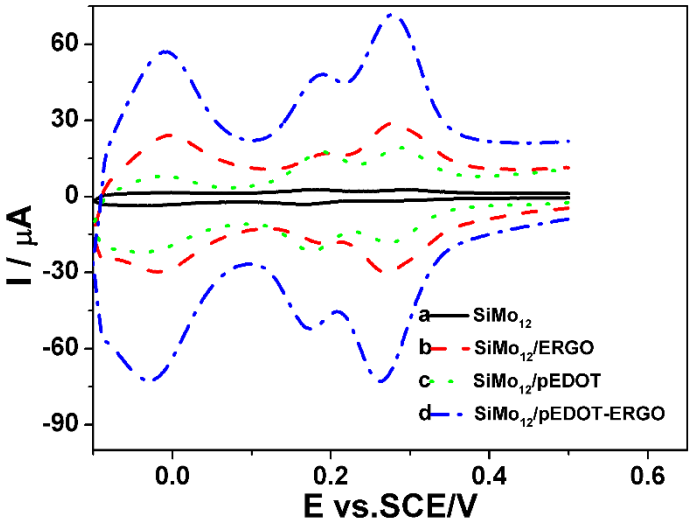

Figure 4. Cyclic voltammograms of a modified ITO with different modifiers including (a) $SiMo_{12}$, (b) $SiMo_{12}$/ERGO, (c) $SiMo_{12}$/pEDOT, and (d) $SiMo_{12}$/pEDOT-ERGO in 0.1 M sulphuric solution at 50 mV s^{-1}, respectively.

We calculated the surface coverage (Γ^*) of $SiMo_{12}$ immobilized on electrode surfaces based on the equation:

$$\Gamma^* = 4i_p RT / n^2F^2vA \quad (2)$$

where i_p is the peak current (A) measured at a slow voltammetric scan rate, A is the surface area of ITO electrode (cm^2) and all other symbols have their usual meanings [38]. Taking the second redox peaks for instance, the calculated Γ^* of $SiMo_{12}$ for the $SiMo_{12}$/ERGO was 2.16×10^{-9} mol cm^{-2} , which is evidently higher than that obtained from the $SiMo_{12}$ modified electrode (1.96×10^{-10} mol cm^{-2}). It can be concluded that the ERGO has a higher active area and has been stably immobilized on the surface of electrode. Moreover, the Γ^* of $SiMo_{12}$ for the $SiMo_{12}$/pEDOT amounts to 1.44×10^{-9} mol cm^{-2}. The result is not surprising because the pEDOT is positively charged and combined with $SiMo_{12}$ through electrostatic interaction. When the ERGO was doped into pEDOT, the surface coverage of $SiMo_{12}$ for the $SiMo_{12}$/pEDOT-ERGO reaches about 5.38×10^{-9} mol cm^{-2}. Clearly, the existence of pEDOT-ERGO further enlarges the Γ^* of $SiMo_{12}$. This finding proves that the pEDOT-ERGO film offers the maximum active area. Besides that, the opposite charge of the pEDOT chains also improves the amount of $SiMo_{12}$ on the film. All the superiorities of the $SiMo_{12}$/pEDOT-ERGO could be attributed to the synergy between the ERGO and pEDOT.

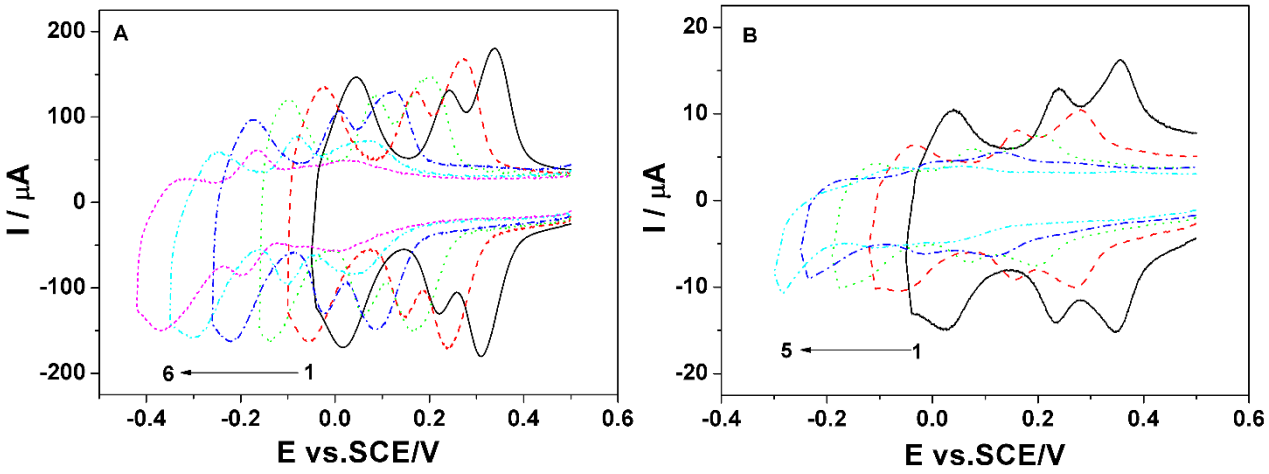

Figure 5. The CVs of (A) $SiMo_{12}$/pEDOT-ERGO/ITO electrode and (B) $SiMo_{12}$/ERGO at different pH solution. Scan rate: 50 mVs^{-1}

The influence of solution pH on $SiMo_{12}$/pEDOT-ERGO/ITO was investigated. From Fig.5A, the redox peak potentials all systematically shift with the pH and the peak currents gradually decrease. It could be elucidated by the fact that the electrochemical reduction process of $SiMo_{12}$ was accompanied by proton transfer to maintain charge neutrality.

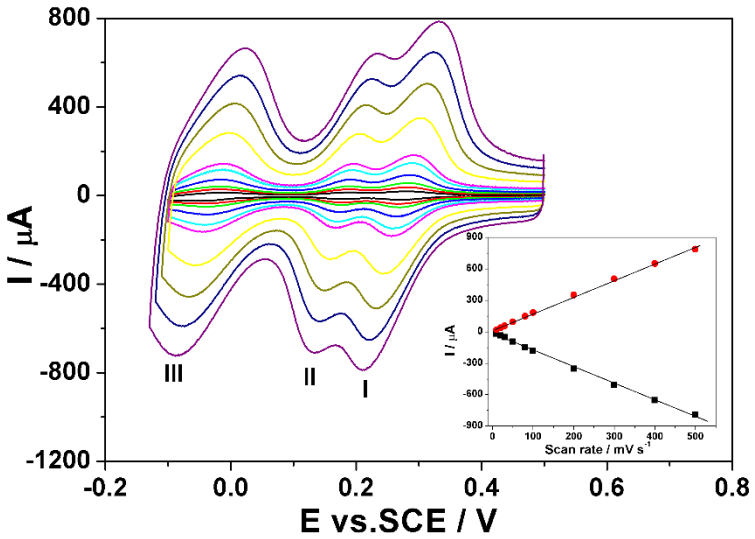

Figure 6. Cyclic voltammograms of the $SiMo_{12}$/pEDOT-ERGO/ITO electrode 0.1 M sulphuric solution at different scan rates (curves from inside to outside: 10, 20,30,50, 80, 100, 200, 300, 400 and 500 mV s^{-1}). The inset shows plots of the cathodic and anodic peak current of the first couple waves against scan rates.

Compared to proton, the slower transfer rate of larger cations[39] is the main reason for the change of current when pH increases. The more negative reduction potentials can be explained by the Nernst equation[40]. For comparison, the cyclic voltammetry of the $SiMo_{12}$/ERGO/ITO in different pH value solution is also presented. As can be seen in Fig.5B, similar results can be noticed. But the electrode response decreases sharply with the solution pH. The redox peaks of $SiMo_{12}$/ERGO come to disappear

at higher pHs than 4.0. Even though the pH value reaches 6, the redox peaks of $SiMo_{12}$/pEDOT-ERGO can be observed obviously. This indicates that the modified electrode shows significant stability in neutral solution, which could be attributed to the promoting effect of pEDOT on the stability of $SiMo_{12}$.

Fig.6 displays the cyclic voltammetry curves of $SiMo_{12}$/pEDOT-ERGO/ITO at different scan rates. Three pairs of reversible redox peaks were clearly observed. Obviously, a systematic increase of peak current upon increasing scan rates was observed. The peak currents were proportional to the scan rates (inset of Fig.6), indicating that the $SiMo_{12}$/pEDOT-ERGO/ITO shows a fast, surface-controlled electron transfer behavior[41,42].

3.3 Electrocatalytic activity of composite films

Cyclic voltammetry response of $SiMo_{12}$/pEDOT-ERGO/ITO with different concentrations of $S_2O_8^{2-}$ (0, 0.5, 1.0, 1.5 and 2.0 mM) in 0.1 M H_2SO_4 solutions are given in Fig.7. As shown, an increase in the third reduction peak current is noticed, indicating that $SiMo_{12}$ exhibits great electrocatalytic activity for the reduction of $S_2O_8^{2-}$. From the inset of Fig.7, it is clear that the progressive increase of the reduction peak currents increase linearly with the increase of $S_2O_8^{2-}$ concentration, demonstrating that the concentration of $S_2O_8^{2-}$ could be determined on $SiMo_{12}$/pEDOT-ERGO the modified electrode.

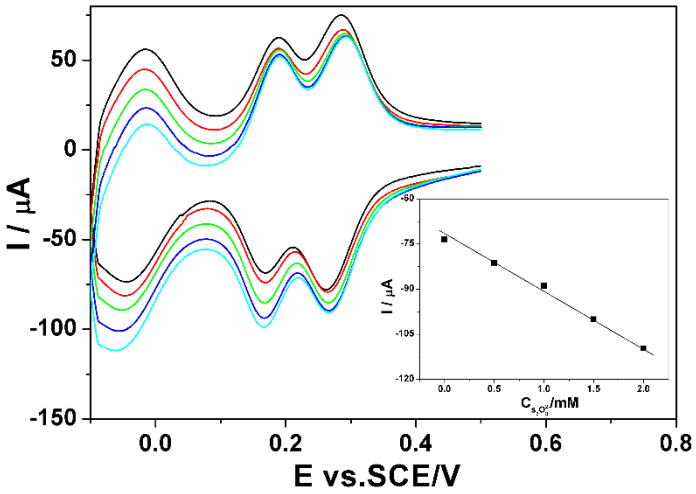

Figure 7. CV curves of $SiMo_{12}$/pEDOT-ERGO/ITO in 0.1 M H_2SO_4 solutions at scan rate 50 mV s^{-1} in the presence of different concentration of $S_2O_8^{2-}$. Inset plot of catalytic current vs. $S_2O_8^{2-}$ concentration.

Amperometry was performed to examine the sensitivity and response time of the $SiMo_{12}$/pEDOT-ERGO/ITO for detection of $S_2O_8^{2-}$. Fig. 8A displays the typical *i-t* curve of the modified electrode with successively spiking 2.5×10^{-3} M $S_2O_8^{2-}$ to 0.1M H_2SO_4 at a fix potential of -0.1 V. A sensitive sensing current signal was obtained when $S_2O_8^{2-}$ is added, which enhances rapidly within 6s. The calibration plot of the response current against the concentration of $S_2O_8^{2-}$ was linear in the range from 1.5×10^{-6} to 1.32×10^{-4} M. The linear equation is I (μA) = -0.21997C (μM) – 1.99339, with regression coefficient value of 0.99987. The detection limit is 0.48 μM and the sensitivity is obtained to be 0.22 μA

μM^{-1} (*S*/*N*=3). Compared with some other reports summarized in Table 1, the $SiMo_{12}$/pEDOT-ERGO modified electrode presents comparable or even superior analytical performance, which is related to the combination effect of $SiMo_{12}$, pEDOT and ERGO. More importantly, $SiMo_{12}$/pEDOT-ERGO electrode is more eco-friendly than those using lead and dye, indicating that it is more suitable for detecting $S_2O_8^{2-}$.

Table 1. Comparison of different electrochemical measurements for $S_2O_8^{2-}$ detection.

Electrode	Method	LR [a] (μM)	DOL[b] (μM)	Sensitivity ($\mu A\ \mu M^{-1}cm^{-2}$)	Ref[c]
Prussian blue/PDE [d]	Cyclic voltammetry	50–3000	41.9	-	43
PbPCNF[f]/CC[g]	Amperometry	5–50	1.58	0.5277	6
PBCB[h]/MWCNTs[i]/GCE[e]	Amperometry	10–100	1	0.1245	44
FAD[j]/NiOx/GCE	Amperometry	3–1500	0.38	0.5287	45
RF[k]/GQDs[l]/GCE	Amperometry	1–1000	0.2	0.1497	9
MY[m]/MWCNTs-Chit[n]/GCE	Amperometry	1.0–1000	0.03	-	46
$(CS\text{-}ERGO^{p})_5/(SiMo_{12})_6$/ITO	Amperometry	0.67–30.62	0.05	0.0448	47
$SiMo_{12}$/pEDOT-ERGO/ITO	Amperometry	1.5-132	0.48	0.22	This work

[a] Linearity range, [b] Detection limit, [c] Reference, [d].Platinum disc electrode, [e] Glass carbon electrode, [f] Lead pentacyanonitrosylferrate, [g] Carbon ceramic, [h] Poly brilliant cresyl blue, [i] Multi wall carbon nanotubes, [j] Flavin adenine dinucleotide, [k] Riboflavin, [l] Graphene quantum dots, [m] metanil yellow, [n] multi wall carbon nanotubes-chitosan, [p] Chitosan-electrochemically reduced graphene oxide.

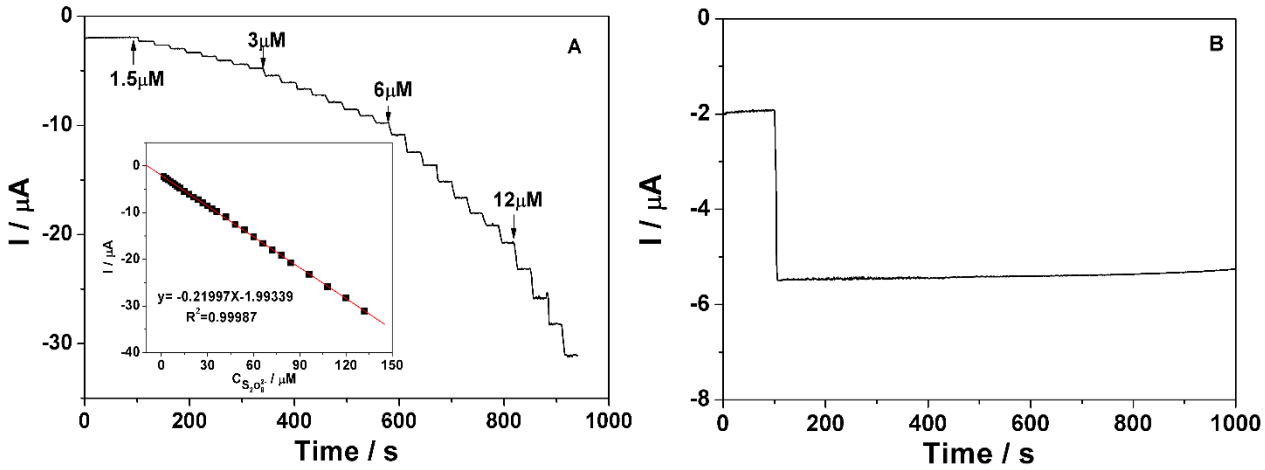

Figure 8. (A) Current-time response of $SiMo_{12}$/pEDOT-ERGO/ITO with successive addition of 2.5×10^{-3} M $S_2O_8^{2-}$ into 0.1 M H_2SO_4. Applied potential: -0.1 V. Insets: The calibration plot of steady-state currents against concentrations of $S_2O_8^{2-}$. (B) The long-term stability response of the $SiMo_{12}$/pEDOT-ERGO/ITO towards the sensing of 15 μM $S_2O_8^{2-}$ under continuous stirring conditions for 15 min.

In order to evaluate the stability of the $SiMo_{12}$/pEDOT-ERGO/ITO, the amperometric response of the modified electrode toward $S_2O_8^{2-}$ during prolonged 15.0 min is shown in Fig. 8B. The corresponding amperometric response of $S_2O_8^{2-}$ As a result, the response retains 95.8% of its initial value, indicating the higher stability of the proposed sensor toward the detection of $S_2O_8^{2-}$.

3.4 Anti-interference performance and preliminary analysis of real samples

The effect of interference from various inorganic ions was recorded by using the amperometric method under successive injections of Na_2SO_3, KCl, $NiCl_2$, $MnCl_2$ and $CoCl_2$ at 200 fold concentrations of $S_2O_8^{2-}$ and the result is shown in Fig. 9. No significant current responses are observed for interfering species. This results reveals that the proposed modified electrode has an excellent selectivity for electrochemical detection of $S_2O_8^{2-}$.

The real samples containing $S_2O_8^{2-}$ were determined by Amperometry using standard addition method. The tap and lake water were used to dilute sulfuric acid and to prepare 5 μM $S_2O_8^{2-}$ solution. The determined concentrations were 5.01 and 4.69 μM. The recoveries of the electrode were 100.2% and 93.8%, correspondingly. These results indicated that the proposed modified electrode in this paper could be employed for the determination of $S_2O_8^{2-}$ in real sample.

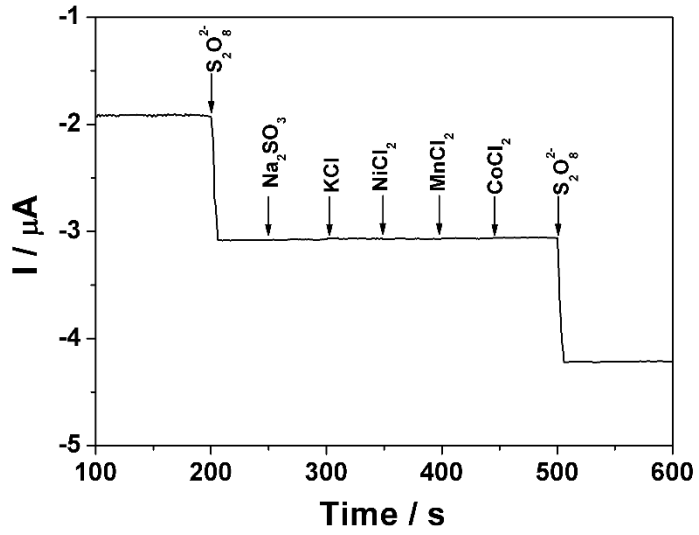

Figure 9. Amperometric response of the $SiMo_{12}$/pEDOT-ERGO/ITO held at -0.1 V in 0.1 M H_2SO_4 during successive addition of $S_2O_8^{2-}$ (5 μM) and 1 mM of Na_2SO_3, KCl, $NiCl_2$, $MnCl_2$ and $CoCl_2$.

4. CONCLUSIONS

In summary, $SiMo_{12}$/pEDOT-ERGO composite modified ITO has been successfully fabricated to detect persulfate. Attributed to the synergistic effect of pEDOT-ERGO and $SiMo_{12}$, the modified electrode exhibits a good current response toward the reduction of persulfate with high sensitivity (~ 0.22 μA μM^{-1}), low detection limit (~0.48 μM) and better selectivity. More complex samples should be used to explore the application of the modified electrode, which will be completed in our future work.

ACKNOWLEDGEMENTS
This work is financially supported by the National Natural Science Foundation of China (Grant No. 21401022, 11475044, 21866001), the Natural Science Foundation of Jiangxi Province (20181BAB213009) and the Open Project Foundation of State Key Laboratory of Nuclear Resources and Environment (East China University of Technology) (Grant No. NRE1811).

References

1. K.C. Lin, T.H. Wu and S.M. Chen , *RSC Adv.*, 5(2015)59946.
2. S. Wacławek, H.V. Lutze, K. Grübel, V.V.T. Padil, M. Černík and D.D. Dionysiou, *Chemical Engineering Journal,* 330(2017)44.
3. A. Baalbaki, N. Zein Eddine, S. Jaber, M. Amasha and A. Ghauch, *Talanta,* 178(2018)237.
4. I.M. Kolthoff and R. Woods, *J. Am. Chem. Soc.,* 88 (1966)1371.
5. L. Zhao, S. Yang, L. Wang, C. Shi, M. Huo and Y. Li, *J. Environ. Sci.,* 31(2015)235.
6. R. Hackam and L. Altcheh, *Electroanalysis,* 20(2008)2370.
7. Z. Savari, S. Soltanian, A. Noorbakhsh, A. Salimi, M. Najafi and P. Servati, *Sens. Actuators, B,* 176(2013)335.
8. M. Roushani and E. Karami, *Electroanalysis,* 26(2014)1761.
9. M. Roushani and Z. Abdi, *Sens. Actuators, B,* 201(2014)503-510.
10. L. Kang, H. Ma, Y. Yu, H. Pang, Y. Song and D. Zhang, *Sens. Actuators, B,* 177(2013)270.
11. W.H. Guo, L. Xu, B. Xu, Y. Yang, Z. Sun and S. Liu, *J. Appl. Electrochem.,* 39(2009)647.
12. H. Ma, Y. Gu, Z. Zhang, H. Pang, S. Li and K. Lu, *Electrochim. Acta,* 56(2011)7428.
13. C. Zhou, S. Li, W. Zhu, H. Pang and H. Ma, *Electrochim. Acta,* 113(2013)454.
14. S. Herrmann, C. Ritchie and C. Streb, *Dalton Trans.,* 44(2015)7092.
15. Y. Ji, L. Huang, J. Hu, C. Streb and Y.F. Song, *Energy Environ. Sci.,* 8(2015)776.
16. M. Zhou, L.P. Guo, F.Y. Lin and H.X. Liu, *Anal. Chim. Acta,* 587(2007)124.
17. A.Z. Ernst, S. Zoladek, K. Wiaderek, J.A. Cox, A. Kolary-Zurowska, K. Miecznikowski and P.J. Kulesza, *Electrochim. Acta,* 53(2008)3924.
18. Y. Shao, J. Wang, H. Wu, J. Liu, I.A. Aksay and Y. Lin, *Electroanalysis,* 22(2010)1027.
19. J. Xu, Y. Wang and S. Hu, *Microchim. Acta,* 184(2017)1.
20. H. Li, S. Pang, X. Feng, K. Mullen and C. Bubeck, *Chem. Commun.* 46(2010)6243
21. H. Li, S. Pang, S. Wu, X. Feng, Müllen K. and Bubeck C, *J. Am. Chem. Soc.,* 133(2011)9423.
22. S. Wang, H. Li, S. Li, F. Liu, D. Wu, X. Feng and L. Wu, *Chem. Eur. J.,* 19(2013)10895.
23. Z. Ma, Y. Qiu, H. Yang, Y. Huang, J. Liu, Y. Lu, C. Zhang and P. Hu, *ACS Appl. Mater. Interfaces,* 7(2015)22036.
24. Ö.A. Yokuş, F. Kardaş, O. Akyıldırım, T. Eren, N. Atar and M.L. Yola, *Sens. Actuators, B,* 233(2016)47.
25. M. Jiao, Z. Li, Y. Li, M. Cui and X. Luo, *Microchim. Acta,* 185(2018)249.
26. R. Agarwal and M.K. Sharma, *Electrochim. Acta,* 224(2017)496-502.
27. W.J. Hong, Y.X.Xu, G.W. Lu, C. Li, G.Q. Shi, *Electrochem. Commun.,* 10(2008)1555.
28. G.X. Wang, Y. Qian, X.X. Cao, X.H. Xia, *Electrochem. Commun.,* 20 (2012) 1–3.
29. D.C. Marcano, D.V. Kosynkin, J.M. Berlin, A. Sinitskii, Z.Z. Sun, A. Slesarev, L.B. Alemany, W. Lu and J.M. Tour, ACS NANO, 4(2010)4806.
30. C. Rocchiccioli-Deltcheff, M. Fournier, R. Franck and R. Thouvenot, *Inorg. Chem.,* 22(1983)207.
31. J. Zhang, D.P. Burt, A.L. Whitworth, D. Mandler and R. Unwin, *Phys. Chem. Chem. Phys.,* 11(2009)3490.
32. L. Lu, O. Zhang, J. Xu, Y. Wen, X. Duan, H. Yu, L. Wu and T. Nie, *Sens. Actuators, B,* 181(2013)567.
33. T. Lindfors, A. Österholm, J. Kauppila and M. Pesonen, *Electrochim. Acta,* 110(2013)428.
34. D. Buttry and A. Bard, Electroanalytical chemistry, Marcel Dekker, New York, 1991, vol. 17.
35. M.Y. Emran, M.A. Shenashen, A.A. Abdelwahab, M. Abdelmottaleb, M. Khairy and S. A. El-Safty, *Electrocatalysis,* 9 (2018)514.
36. P. Zuman and R. N. Adams, M. Dekker, New York, 1969, vol. xiii, p. 402.
37. M.Y. Emran, M.A. Shenashen, A.A. Abdelwahab, M. Abdelmottaleb and S.A. El-Safty, *New J. Chem.*, 42(2018)5037.

38. Z.F. Li, J.H. Chen, D.W. Pan, W.Y. Tao, L.H. Nie, S.Z. Yao. *Electrochim. Acta,* 51(2006)4255.
39. C.M.A. Brett and A.M.O. Brett. Electrochemistry: Principles, Methods, and Applications, (1993)Oxford Press.
40. J. Wang, Analytical Electrochemistry, (1994)VCH, New York.
41. Z.H. Wang, Q.H. Han, J.F. Xia, L. Xia, S. Bi, G.Y. Shi, F.F. Zhang, Y.Z. Xia, Y.H. Li and L.H. Xia, *J. Electroanal. Chem.*,726(2014)107.
42. S.S. Hassana, Y.P. Liua, Sirajuddinb, A.R. Solangi, A.M. Bonda and J. Zhanga, *Anal. Chim. Acta,* 803(2013)41.
43. M.F.D. Oliveira, R.J. Mortimer and N.R. Stradiotto, *Microchem. J,* 64(2000)155.
44. K.C. Lin, J.Y. Huang and S.M. Chen , *Int. J. Electrochem. Sci.,* 7(2012)9161.
45. A. Salimi, A. Noorbakhsh and A. Semnani, *J. Solid State Electrochem.,* 15(2011)2041.
46. M. Roushani, Z. Rahmati and B.Z. Dizajdizi, *J. Electroanal. Chem.*, 847(2019)113192.
47. W.H. Guo, X.L. and Tong and S.B. Liu, *Electrochim. Acta,* 173(2015)540-550.